

Figure 6 Variation of return loss with frequency for $l_n = 40$ mm, $p_n = 10$ mm, and $s = 6$ mm

good agreement with experimental result [9], and the bandwidth of the antenna is found to be 32.5%. From Figure 7, it is observed that the directivity of ESPA decreases with frequency and the direction of maximum radiation are shifted by 5° from the broad side direction. Thus, from the above discussion it is found that the antenna length (l) controls the higher resonant frequency, while the notch controls the lower resonant frequency and matching condition. Similar experimental observations were also observed by Yang et al. [9].

5. CONCLUSION

It may be concluded that due to dual resonance nature ESPA shows a wide-bandwidth characteristic. It is also concluded that the notch length, width, and position are important parameters in controlling the achievable bandwidth.

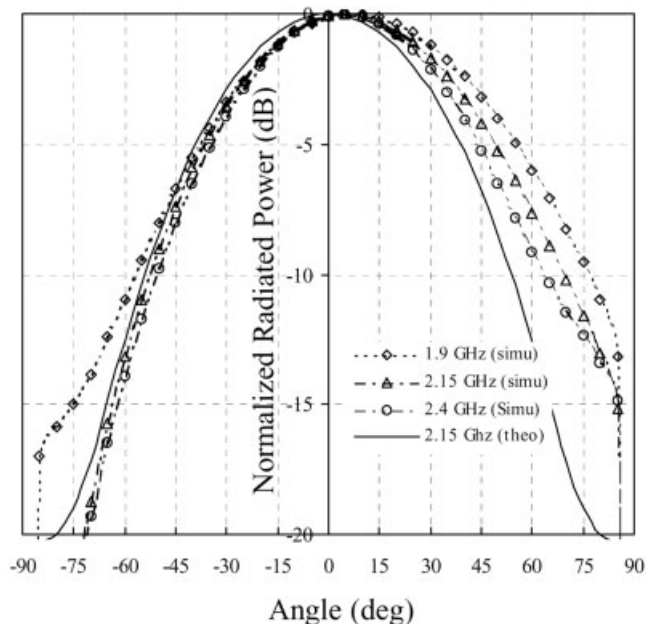


Figure 7 E-plane radiation patterns at different frequencies

ACKNOWLEDGMENTS

VKP is thankful to the University Grant Commission, New Delhi, for providing him a Senior Research Fellowship. The authors are also thankful to DRDO for providing financial assistance for the IE3D software.

REFERENCES

1. K.-L. Wong, Compact and broadband microstrip antennas, Wiley, New York, 2002, pp. 232–273.
2. K.F. Lee and W. Chen, Advances in microstrip and printed antennas, Wiley, New York, 1997, pp. 53–62.
3. K.F. Lee, K.M. Luk, K.F. Tong, S.M. Shum, T. Huynh, and R.Q. Lee, Experimental and simulation studies of the coaxially fed U-slot rectangular patch antenna, Proc Inst Elec Eng 144 (1997), 354–358.
4. T. Huynh and K.F. Lee, Single-layer single-patch wideband microstrip antenna, Electron Lett 31 (1995), 1310, 1311.
5. J.Y. Sze and K.L. Wong, Single-layer single-patch broadband rectangular microstrip antenna, Microwave Opt Technol Lett 22 (1999), 234–236.
6. K.M. Luk, L.K. Au Yeung, C.L. Mak, and K.F. Lee, Circular patch antenna with an L-shaped probe, Microwave Opt Technol Lett 20 (1999), 256, 257.
7. B.L. Ooi and Q. Shen, A novel E-shaped broadband microstrip patch antenna, Microwave Opt Technol Lett 27 (2000), 348–352.
8. K.L. Wong and W.H. Hsu, A broad-band rectangular patch antenna with a pair of wide slits, IEEE Trans Antennas Propag 49 (2001), 1345–1347.
9. F. Yang, X.X. Zhang, X. Ye, and R.S. Yahya, Wide-band E-shaped patch antennas for wireless communications, IEEE Trans Antennas Propag 49 (2001), 1094–1100.
10. E.S. Neves, M.V.T. Heckler, R. Schildberg, J.C. Da, S. Lacava, and L. Cividanes, Single-layer rectangular patch antenna with two pairs of parallel slits, Microwave Opt Technol Lett 37 (2003), 355–359.
11. G. Yuehe, K.P. Esselle, and T.S. Bird, A broadband E-shaped patch antenna with a microstrip-compatible feed, Microwave Opt Technol Lett 42 (2004), 111, 112.
12. F.E. Terman, Electronic and radio engineering, Kogakusha, Tokyo, 1955, pp. 15–73.
13. X.X. Zhang and F. Yang, Study of a slit cut on a microstrip antenna and its applications, Microwave Opt Technol Lett 18 (1998), 297–300.
14. I. Bahl, Lumped elements for RF and microwave circuits, Artech House, Boston, 2003, pp. 456–459.
15. C.A. Balanis, Antenna theory analysis and design, 2nd ed., Wiley, New York, 1997, pp. 728–746.

© 2006 Wiley Periodicals, Inc.

MODELING ABSORPTION OF ROUGH INTERFACE BETWEEN DIELECTRIC AND CONDUCTIVE MEDIUM

Xiaoxiong Gu,¹ Leung Tsang,¹ Henning Braunsch,² and Peng Xu³

¹ University of Washington
Seattle, WA 98195-2500

² Intel Corporation
Chandler, AZ

³ Wuhan University
Wuhan, China

Received 5 May 2006

ABSTRACT: The effects of a random rough surface between dielectric and lossy conductive medium on power absorption are analyzed by considering incident plane waves impinging on the interface. We use two methods to formulate and solve the 2-D problem: the two-media small perturbation method to second order (SPM2) and the numerical system

transfer operator matrix method, referred to as T-matrix method. The two methods are in agreement within the regimes of validity. The results show significant difference between absorption of a rough surface and that of a smooth surface. Surface fields are further examined numerically. © 2006 Wiley Periodicals, Inc. Microwave Opt Technol Lett 49: 7–13, 2007; Published online in Wiley InterScience (www.interscience.wiley.com). DOI 10.1002/mop.22023

Key words: conductors; perturbation methods; T-matrix method; rough surfaces

1. INTRODUCTION

The roughness of the interfaces between metal and dielectric layers, especially in microelectronic packaging based on organic materials, is often used to facilitate the adherence of the copper structures to the dielectrics. Since the speed of interconnects is now in the multi-GHz region, the roughness of the surface can have significant effects, especially on conductor loss, which can be detrimental for insertion loss limited designs. Therefore, in order to guide substrate technology research and development, it is imperative to understand these effects in detail. Presently the common results for quantifying the impact of conductor surface roughness on Ohmic loss are due to Morgan's classic paper [1] and the Hammerstad and Bekkadal formula [2]. Their model is also adopted in many of the existing commercial design tools. However, Morgan only used a periodic ridge structure as rough surface which may misrepresent the roughness-induced loss.

The underlying physics is focused on the analysis of the interactions of electromagnetic waves with the rough surface. Research by Sanderson [3] shows that the Rayleigh-Rice perturbation technique [4, 5] gives good results for periodic surface roughness when slopes are small to moderate. Rytov [6] and Tsang et al. [7] further speculate that this may also be true for random or non-periodic roughness. More recently, we applied Rayleigh-Rice perturbation technique of second order to a random rough surface and derived a closed-form formula of power absorption enhancement factor [8]. Similar to Morgan's assumption, we enforced a constant magnetic field as the boundary condition and only solved the fields in the conductor as a one-medium problem.

In this paper, we extend the SPM2 approach to two-media studies including both the dielectric region and conductor region. The rough interface is modeled by the characteristics of RMS height, correlation length, and correlation function. The absorption is calculated by two methods: the analytic small perturbation method to second order (SPM2) and the numerical system transfer operator matrix (T-matrix) method. The results of absorption based on SPM2 are in terms of the spectral density of the random rough surface. Furthermore, instead of assuming constant magnetic fields on the rough interface, the new methods in this paper take into account both dielectric region and conductor region by considering a plane wave impinging on the interface.

Characterization of random rough surfaces is discussed in Section 2. Section 3 and Section 4 include formulation and solution of analytic and numerical methods. Numerical results are illustrated in Section 5.

2. RANDOM ROUGH SURFACES

For a 2-D problem of random rough surface, the height function $f(x)$ is treated as a stationary Gaussian random process. The two point ensemble average of the random process is

$$\langle f(x_1)f(x_2) \rangle = h^2 C(|x_1 - x_2|), \quad (1)$$

where $h^2 C(x)$ is the correlation function. Two common correlation functions are the Gaussian correlation function with $C(x)$

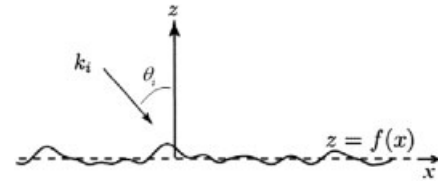


Figure 1 A plane wave impinging on a rough surface with incident angle

$= \exp(-x^2/l^2)$ and exponential correlation function with $C(x) = \exp(-|x|/l)$, where l is the correlation length. The exponential correlation profile appears significantly rougher than that for the Gaussian correlation function. In generating the roughness profiles [9], we use the spectral density function $W(k_x)$ which is the Fourier transform of the correlation function. The spectral density of the Gaussian correlation function is given by $W(k_x) = \frac{h^2 l}{2\sqrt{\pi}} \exp(-k_x^2 l^2/4)$ and that of the exponential correlation function by $W(k_x) = \frac{h^2 l}{\pi(1 + k_x^2 l^2)}$ [10].

3. ANALYTIC SMALL PERTURBATION METHOD

3.1. Two-Media Formulation

Consider a random rough surface profile $z = f(x)$, as shown in Figure 1. In a 2-D transverse magnetic (TM) problem, the magnetic field in the \hat{y} direction is denoted as ψ . Let ψ and ψ_1 be the magnetic fields in the upper dielectric and lower conductor region, respectively. A plane wave with incident angle θ_i is expressed as follows:

$$\psi_{\text{inc}}(\vec{r}) = \exp(ik_{ix}x - ik_{iz}z), \quad (2)$$

where $k_{ix} = k \sin\theta_i$, $k_{iz} = k \cos\theta_i$, and k is the wave number in the dielectric.

Since the tangential electric and magnetic fields are continuous at the boundary, namely, $\psi(\vec{r}) = \psi_1(\vec{r})$ and $\hat{n} \cdot \nabla\psi(\vec{r}) = \frac{\epsilon}{\epsilon_1} \hat{n} \cdot \nabla\psi_1(\vec{r})$ where ϵ and ϵ_1 are the permittivity of the dielectric and conductor, we can define surface field unknowns as follows:

$$a(x) = \psi_1(x, f(x)), \quad (3)$$

$$b(x) = \sqrt{1 + \left(\frac{df}{dx}\right)^2} [\hat{n} \cdot \nabla\psi_1(\vec{r})]_{z=f(x)}. \quad (4)$$

Applying the extinction theorem to both dielectric and conductor regions [11] gives

$$\psi_{\text{inc}}(\vec{r}') + \int_S dx \left[a(x) \sqrt{1 + \left(\frac{df}{dx}\right)^2} \hat{n} \cdot \nabla g(\vec{r}, \vec{r}') - g(\vec{r}, \vec{r}') \frac{\epsilon}{\epsilon_1} b(x) \right] = 0 \quad \text{for } z' < f(x'), \quad (5)$$

$$\int_S dx \left[a(x) \sqrt{1 + \left(\frac{df}{dx}\right)^2} \hat{n} \cdot \nabla g_1(\vec{r}, \vec{r}') - g_1(\vec{r}, \vec{r}') b(x) \right] = 0 \quad \text{for } z' > f(x'), \quad (6)$$

where $g(\vec{r}, \vec{r}')$ and $g_1(\vec{r}, \vec{r}')$ are the plane wave representation of the Green's function in the two regions:

$$g(\vec{r}, \vec{r}') = \frac{i}{4\pi} \int_{-\infty}^{\infty} dk_x \frac{1}{k_z} \exp(ik_x(x'-x) + ik_z|z'-z|), \quad (7)$$

$$g_1(\vec{r}, \vec{r}') = \frac{i}{4\pi} \int_{-\infty}^{\infty} dk_x \frac{1}{k_{1z}} \exp(ik_x(x'-x) + ik_{1z}|z'-z|). \quad (8)$$

Here $k_z = \sqrt{k^2 - k_x^2}$, $k_{1z} = \sqrt{k_1^2 - k_x^2}$, $k_1 = (1 + i)/\delta$, δ is the skin depth ($\delta = \sqrt{2/(\pi\omega\mu\sigma)}$), σ is the conductivity of the conductor, μ is its magnetic permeability, and $\omega = 2\pi f$ is the angular frequency.

We use a second order perturbation method, letting $A(k_x)$ and $B(k_x)$ be the Fourier transforms of the field unknowns $a(x)$ and $b(x)$.

3.2. Zeroth-Order, First-Order, and Second-Order Solution

Balancing (5) and (6) to second order after substituting (7) and (8) gives the solutions of zeroth, first and second order as follows.

The zeroth-order solution is:

$$A^{(0)}(k_x) = \tilde{A}_0 \delta(k_x - k_{ix}), \quad (9)$$

$$B^{(0)}(k_x) = \tilde{B}_0 \delta(k_x - k_{ix}), \quad (10)$$

where

$$\tilde{A}_0 = \frac{2k_{iz}\epsilon_1}{k_{iz}\epsilon_1 + \epsilon k_{1zi}}, \quad (11)$$

$$\tilde{B}_0 = \frac{-2ik_{1zi}k_{iz}\epsilon_1}{k_{iz}\epsilon_1 + \epsilon k_{1zi}}, \quad (12)$$

and $k_{1zi} = \sqrt{k_1^2 - k_x^2}$ and $\delta(k_x)$ is the Dirac delta function.

The first-order solution is:

$$A^{(1)}(k_x) = \tilde{A}_1(k_x) F(k_x - k_{ix}), \quad (13)$$

$$B^{(1)}(k_x) = \tilde{B}_1(k_x) F(k_x - k_{ix}), \quad (14)$$

where $F(k_x)$ is the Fourier transform of $f(x)$ and $\tilde{A}_1(k_x)$ and $\tilde{B}_1(k_x)$ obey the following two simultaneous equations:

$$-ik_z \tilde{A}_1(k_x) + \frac{\epsilon}{\epsilon_1} \tilde{B}_1(k_x) = -k_z^2 \tilde{A}_0 - k_x(k_x - k_{ix}) \tilde{A}_0 - \frac{\epsilon}{\epsilon_1} ik_z \tilde{B}_0, \quad (15)$$

$$ik_{1z} \tilde{A}_1(k_x) + \tilde{B}_1(k_x) = -k_{1z}^2 \tilde{A}_0 - k_x(k_x - k_{ix}) \tilde{A}_0 + ik_{1z} \tilde{B}_0. \quad (16)$$

For the second-order solution, we only need to calculate the ensemble average of $A^{(2)}$ and $B^{(2)}$:

$$\langle A^{(2)}(k_x) \rangle = \tilde{A}_2 \delta(k_x - k_{ix}), \quad (17)$$

$$\langle B^{(2)}(k_x) \rangle = \tilde{B}_2 \delta(k_x - k_{ix}), \quad (18)$$

where \tilde{A}_2 and \tilde{B}_2 obey two simultaneous equations:

$$\begin{aligned} -ik_{iz} \tilde{A}_2 + \frac{\epsilon}{\epsilon_1} \tilde{B}_2 = & \\ -i \frac{k_{iz}^3}{2} \tilde{A}_0 \int_{-\infty}^{\infty} dk_x W(k_x - k_{ix}) - ik_{ix} k_{iz} \tilde{A}_0 \int_{-\infty}^{\infty} dk_x W(k_x - k_{ix})(k_x - k_{ix}) & \\ - k_{iz}^2 \int_{-\infty}^{\infty} dk_x W(k_x - k_{ix}) \tilde{A}_1(k_x) - k_{ix} \int_{-\infty}^{\infty} dk_x (k_{ix} - k_x) W(k_x & \\ - k_{ix}) \tilde{A}_1(k_x) & \\ + \frac{\epsilon}{\epsilon_1} \frac{k_{iz}^2}{2} \tilde{B}_0 \int_{-\infty}^{\infty} dk_x W(k_x - k_{ix}) - \frac{\epsilon}{\epsilon_1} ik_{iz} \int_{-\infty}^{\infty} dk_x W(k_x - k_{ix}) \tilde{B}_1(k_x), & \end{aligned} \quad (19)$$

$$\begin{aligned} ik_{1zi} \tilde{A}_2 + \tilde{B}_2 = & \\ i \frac{k_{1zi}^3}{2} \tilde{A}_0 \int_{-\infty}^{\infty} dk_x W(k_x - k_{ix}) + ik_{ix} k_{1zi} \tilde{A}_0 \int_{-\infty}^{\infty} dk_x W(k_x - k_{ix})(k_x - k_{ix}) & \\ - k_{1zi}^2 \int_{-\infty}^{\infty} dk_x W(k_x - k_{ix}) \tilde{A}_1(k_x) - k_{ix} \int_{-\infty}^{\infty} dk_x (k_{ix} - k_x) W(k_x & \\ - k_{ix}) \tilde{A}_1(k_x) & \\ + \frac{k_{1zi}^2}{2} \tilde{B}_0 \int_{-\infty}^{\infty} dk_x W(k_x - k_{ix}) + ik_{1zi} \int_{-\infty}^{\infty} dk_x W(k_x - k_{ix}) \tilde{B}_1(k_x). & \end{aligned} \quad (20)$$

3.3. Coherent and Incoherent Scattered Field

The total scattered fields ψ_s can be determined using the extinction theorem [11]:

$$\psi_s(\vec{r}') = \int_S dx \left[a(x) \sqrt{1 + \left(\frac{df}{dx}\right)^2} \hat{n} \cdot \nabla g(\vec{r}, \vec{r}') - g(\vec{r}, \vec{r}') \frac{\epsilon}{\epsilon_1} b(x) \right] \text{ for } z' > f(x'). \quad (21)$$

To calculate absorption, we need to sum the contribution from coherent and incoherent scattered fields respectively. In the case of 2-D rough surface, the coherent scattering occurs at zeroth order and second order while incoherent scattering occurs at first order.

Using the aforementioned solution of surface fields gives the coherent solution to second order. The zeroth-order coherent scattered field is

$$\psi_s^{(0)}(k_x) = \tilde{\psi}_s^{(0)} \delta(k_x - k_{ix}), \quad (22)$$

where

$$\tilde{\psi}_s^{(0)} = \frac{\epsilon_1 k_{iz} - \epsilon k_{1zi}}{\epsilon_1 k_{iz} + \epsilon k_{1zi}} \quad (23)$$

The second-order coherent scattered field is

$$\langle \psi_s^{(2)}(k_x) \rangle = \tilde{\psi}_s^{(2)} \delta(k_x - k_{ix}), \quad (24)$$

where

$$\begin{aligned} \tilde{\psi}_s^{(2)} = & -\frac{k_{ix}^2 h^2}{2} \tilde{\psi}_s^{(0)} - \frac{ik_{iz}}{2} \int_{-\infty}^{\infty} dk_x \tilde{A}_1(k_x) W(k_{ix} - k_x) \\ & - \frac{k_{ix}}{2k_{iz}} \int_{-\infty}^{\infty} dk_x \tilde{A}_1(k_x) W(k_{ix} - k_x) i(k_{ix} - k_x) \\ & + \frac{\tilde{A}_2}{2} - \frac{\varepsilon}{2\varepsilon_1} \int_{-\infty}^{\infty} dk_x \tilde{B}_1(k_x) W(k_{ix} - k_x) - \frac{i\varepsilon}{2k_{iz}\varepsilon_1} \tilde{B}_2, \end{aligned} \quad (25)$$

The solution of first-order incoherent scattered field is

$$\psi_s^{(1)}(k_x) = \tilde{\psi}_s^{(1)}(k_x) F(k_x - k_{ix}), \quad (26)$$

where

$$\tilde{\psi}_s^{(1)}(k_x) = \frac{i}{2k_z} \left[-k_z^2 \tilde{A}_0 - k_x(k_x - k_{ix}) \tilde{A}_0 - ik_z \tilde{A}_1(k_x) + ik_z \frac{\varepsilon}{\varepsilon_1} \tilde{B}_0 - \frac{\varepsilon}{\varepsilon_1} \tilde{B}_1(k_x) \right]. \quad (27)$$

3.4. Power Absorption Due to Coherent and Incoherent Scattering

In the 2-D problem, power scattered per unit area in the \hat{z} direction can be calculated by using Poynting's theorem:

$$\bar{S}_s \cdot \hat{z} = \text{Re} \left[\frac{i}{2\omega\varepsilon} \left(\psi_s \frac{\partial}{\partial z} \psi_s^* \right) \right]. \quad (28)$$

Since the total incident power per unit area in the $-\hat{z}$ direction is $\bar{S}_{\text{inc}} \cdot (-\hat{z}) = \eta \cos\theta/2$, the emissivity of the lossy conductive medium is given by

$$\begin{aligned} e_v = & 1 - \frac{\langle \bar{S}_s \cdot \hat{z} \rangle_{\text{coh}}}{\bar{S}_{\text{inc}} \cdot (-\hat{z})} - \frac{\langle \bar{S}_s \cdot \hat{z} \rangle_{\text{incoh}}}{\bar{S}_{\text{inc}} \cdot (-\hat{z})} \\ = & 1 - |\tilde{\psi}_s^{(0)}|^2 - 2\text{Re}\{\tilde{\psi}_s^{(0)} \tilde{\psi}_s^{(2)*}\} - \frac{1}{k \cos\theta_1} \\ & \int_{-k}^k dk_x |\tilde{\psi}_s^{(1)}(k_x)|^2 W(k_x - k_{ix}) k_z, \end{aligned} \quad (29)$$

where the second and the third term represent coherent reflectivity and the last term is incoherent reflectivity. Note that as a result of the analytic derivation, the limits of integration in (25) are from $-\infty$ to ∞ , whereas in the last term of (29) they are from $-k$ to k .

On the other hand, for a surface with length $-L/2$ to $L/2$ in the \hat{x} direction, the average power absorption can be calculated directly by using the fields on the surface

$$\begin{aligned} P_a = & -\int dS (\bar{S} \cdot \hat{n}) = -\frac{L}{2} \text{Re} \left\{ \frac{1}{i\omega\varepsilon_1} \int_{-\infty}^{\infty} dk_x \int_{-\infty}^{\infty} dk'_x \right. \\ & \left. \frac{\sin((k'_x - k_x)L/2)}{(k'_x - k_x)L/2} \langle A^*(k_x) B(k'_x) \rangle \right\}. \end{aligned} \quad (30)$$

Putting the solutions of the surface fields into (30) and dividing by the incident power $\eta \cos\theta/2$ gives the absorptivity of the lossy conductive medium:

$$\begin{aligned} a_v = & 1 - \frac{\left| \frac{\varepsilon_1 k_{iz} - \varepsilon k_{1z}}{\varepsilon_1 k_{iz} + \varepsilon k_{1z}} \right|^2}{\left| \frac{\varepsilon_1 k_{iz} - \varepsilon k_{1z}}{\varepsilon_1 k_{iz} + \varepsilon k_{1z}} \right|^2} \\ & - \text{Re} \left\{ \frac{1}{i\omega\varepsilon_1 \eta \cos\theta_1} \int_{-\infty}^{\infty} dk_x \tilde{A}_1^*(k_x) \tilde{B}_1(k_x) W(k_x - k_{ix}) \right\} \\ & - \text{Re} \left\{ \frac{1}{i\omega\varepsilon_1 \eta \cos\theta} (\tilde{A}_2^* \tilde{B}_0 + \tilde{A}_0^* \tilde{B}_2) \right\} \end{aligned} \quad (31)$$

Here η is the wave impedance in the dielectric and the limits of integration are from $-\infty$ to ∞ . We will show e_v and a_v in the following numerical results, proving that SPM2 obeys reciprocity and energy conservation.

3.5. Emissivity of Metal Surface

Next we consider a special case where the lower medium is a highly conductive metal such as copper. On such a metal surface, the RMS height h and correlation length l are in the order of micrometers. The wave length k in the dielectric is in the order of cm^{-1} at microwave frequencies. The incoherent reflectivity is negligibly small because it is in the order of $O(k^3 h^2 l)$.

Also note that $k/|k_x|$ is of order 10^{-4} and $\varepsilon/|\varepsilon_1|$ is of order 10^{-8} . We then calculate the solution of surface fields to the first order of k since k is much smaller than k_1 . The zeroth-order solution remains the same as in (11)–(12). For first-order solution, approximating (15)–(16) by assuming $k_z = \sqrt{k^2 - k_x^2} \approx i|k_x|$ and $k_{ix} \ll |k_x|$ gives

$$\tilde{A}_1(k_x) = \frac{2k_x k_{ix}}{|k_x|}, \quad (32)$$

$$\tilde{B}_1(k_x) = 2k_1(-k_1 + k_{1z}). \quad (33)$$

Approximating (19)–(20) by using (32)–(33) and assuming $W(k_{ix} - k_x) \approx W(k_x)$ gives the second-order solution

$$\tilde{A}_2 = \frac{\varepsilon}{ik_{iz}\varepsilon_1} \tilde{B}_2, \quad (34)$$

$$\tilde{B}_2 = 2ik_1^2 \int_{-\infty}^{\infty} dk_x W(k_x) (-k_1 + k_{1z}). \quad (35)$$

Putting (32)–(35) into (25) gives the second-order scattered field

$$\tilde{\psi}_s^{(2)} = \frac{ik_{ix}^2}{k_{iz}} \int_{-\infty}^{\infty} dk_x \frac{k_x^2}{|k_x|} W(k_x) + \frac{2k}{\cos\theta_1} \int_{-\infty}^{\infty} dk_x W(k_x) (-k_1 + k_{1z}). \quad (36)$$

Note that the first term in $\tilde{\psi}_s^{(2)}$ is purely imaginary. For the integral $\int dk_x$, the integral limit of k_x is of order $1/l$ and is much larger than k .

Next we calculate the emissivity to the first order of k . Approximating (23) by assuming $|k_1| \gg k \sin\theta_1$ gives

$$\tilde{\psi}_s^{(0)} = \frac{k_1 \cos\theta_1 - k}{k_1 \cos\theta_1 + k} \quad (37)$$

Approximating terms in (29) to the first order of k by assuming that $\cos\theta_i$ is not small gives

$$1 - |\tilde{\psi}_s^{(0)}|^2 = \frac{2k\delta}{\cos\theta_i}, \quad (38)$$

$$\text{Re}\{\tilde{\psi}_s^{(0)*}\tilde{\psi}_s^{(2)}\} = \text{Re}\tilde{\psi}_s^{(2)}, \quad (39)$$

Putting (38)–(39) into (29) gives

$$e_v = \frac{2k^2\delta}{k_{iz}} - 2\text{Re}\tilde{\psi}_s^{(2)}, \quad (40)$$

where

$$\text{Re}\tilde{\psi}_s^{(2)} = -\frac{2kh^2}{\cos\theta_i}\text{Re}k_1 + \frac{2k}{\cos\theta_i}\int_{-\infty}^{\infty} dk_x W(k_x)\text{Re}k_{1z}, \quad (41)$$

Here the integral in (41) is convergent because $W(k_x)\text{Re}k_{1z}$ asymptotically approaches $W(k_x)/(\delta^2 k_x)$ as k_x becomes large. So we can extend the limits of integration from $-\infty$ to ∞ . The emissivity of the metal surface becomes

$$e_v = \frac{2k\delta}{\cos\theta_i} + \frac{4kh^2}{\delta\cos\theta_i} - \frac{4k}{\cos\theta_i}\int_{-\infty}^{\infty} dk_x W(k_x)\text{Re}k_{1z}. \quad (42)$$

Dividing (42) by (38) gives the power absorption ratio between rough surface and smooth surface, leading to

$$\frac{P_{\text{a,rough}}}{P_{\text{a,smooth}}} = \frac{e_v}{2k\delta/\cos\theta_i} = 1 + 2\left[\frac{h^2}{\delta^2} - \frac{2}{\delta}\int_{-\infty}^{\infty} dk_x W(k_x)\text{Re}k_{1z}\right]. \quad (43)$$

4. NUMERICAL APPROACH USING T-MATRIX METHOD

To validate the SPM2 results, we use a numerical T-matrix method to compute power absorption as well as magnetic field on the rough surface. We apply the periodic boundary condition with the period L . This is a valid approximation in random rough surface scattering provided that the period contains many peaks and valleys and many correlation lengths, i.e., $L \gg l$ [9]. Using the T-matrix method on (5) and (6) to formulate matrix equations gives

$$\bar{A}\bar{\alpha} + \bar{B}\bar{\beta} = \bar{V}, \quad (44)$$

$$\bar{A}_1\bar{\alpha} = \bar{B}_1\bar{\beta}. \quad (45)$$

In the above two equations, the matrix elements are as follows, assuming S_0 is the rough surface with length L in the \hat{x} direction and x_0 is a point on S_0 :

$$A_{(m+N_m+1)(m'+N_m+1)} = \int_{S_0} dx_0 \exp[-i(k_{xm} - k_{xm'} - k_{ix})x_0 + ik_{zm}f(x_0)]\left(\frac{k_{xm}}{k_{zm}}\frac{df}{dx} + 1\right) \quad (46)$$

$$B_{(m+N_m+1)(m'+N_m+1)} = \int_{S_0} dx_0 \exp[-i(k_{xm} - k_{xm'} - k_{ix})x_0 + ik_{zm}f(x_0)]\frac{\varepsilon}{\varepsilon_1}\frac{i}{k_{zm}}, \quad (47)$$

$$A_{1(m+N_m+1)(m'+N_m+1)} = \int_{S_0} dx_0 \exp[-i(k_{xm} - k_{xm'} - k_{ix})x_0 - ik_{1zm}f(x_0)]\left(\frac{k_{xm}}{k_{1zm}}\frac{df}{dx} - 1\right), \quad (48)$$

$$B_{1(m+N_m+1)(m'+N_m+1)} = \int_{S_0} dx_0 \exp[-i(k_{xm} - k_{xm'} - k_{ix})x_0 - ik_{1zm}f(x_0)]\frac{-i}{k_{1zm}}, \quad (49)$$

$$\bar{V} = \begin{bmatrix} \bar{0}_{N_m \times 1} \\ 2L \\ \bar{0}_{N_m \times 1} \end{bmatrix}, \quad (50)$$

where $k_{xm} = k_{ix} - \frac{2\pi m}{L}$, $k_{xm'} = k_{ix} - \frac{2\pi m'}{L}$, $k_{zm} = \sqrt{k^2 - k_{xm}^2}$, $k_{1zm} = \sqrt{k_1^2 - k_{xm}^2}$, $m = -N_m, -N_m + 1, \dots, N_m - 1, N_m$ and $m' = -N_m', -N_m' + 1, \dots, N_m' - 1, N_m'$.

Surface fields can be further obtained after solving the unknowns $\bar{\alpha}$ and $\bar{\beta}$:

$$a(x_0) = \exp(ik_{ix}x_0) \sum_{m=-N_m}^{N_m} \alpha_m \exp(ik_{xm}x_0), \quad (51)$$

$$b(x_0) = \exp(ik_{ix}x_0) \sum_{m=-N_m}^{N_m} \beta_m \exp(ik_{xm}x_0). \quad (52)$$

Then we can compute the power absorption by the conductor, for a given width w in the \hat{y} direction and length L in the \hat{x} direction.

$$P_{\text{a,rough}} = \frac{w}{2\sigma} \text{Re} \int_{-L/2}^{L/2} dx \psi_1^* \sqrt{1 + \left(\frac{df}{dx}\right)^2} \hat{n} \cdot \nabla \psi_1 = \frac{w}{2\sigma} \text{Re} \sum_{i=1}^{N_s} b_i a_i^* \Delta x. \quad (53)$$

where N_s is the number of discretization elements on the surface.

In the numerical implementation, we take $L = 20l$, $N_m = 30$, and the surface discretization is chosen as $\Delta x = \min\{h/20, l/20, \delta/20\}$. To calculate the average power absorption, we use a Monte-Carlo simulation approach. We generate a large number of realizations of rough profiles. Solving the T-matrix equations we then calculate the absorption ratio for every realization and the average absorption is computed. For the simulation results shown in the next section, 600 realizations are used.

5. RESULTS AND DISCUSSION

5.1. Absorption by Copper Surface Using SPM2

In the following examples, we assume a conductor with the conductivity of pure copper ($\sigma = 5.8 \times 10^7$ S/m) and a dielectric with a relative permittivity of 4.0. The SPM2 results are based on

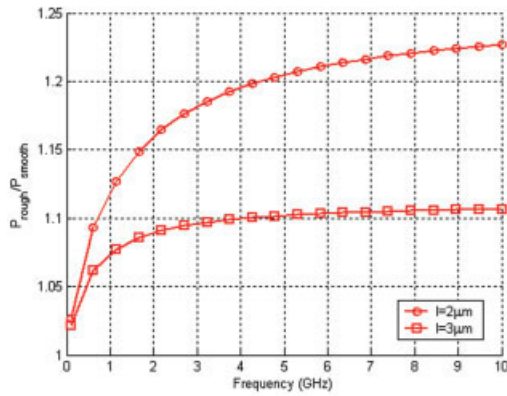


Figure 2 Power absorption ratio as a function of frequency from SPM2: Gaussian correlation function ($h = 1 \mu\text{m}$) with varying correlation length. [Color figure can be viewed in the online issue, which is available at www.interscience.wiley.com]

equations in Sections 3.2–3.4. They are independent of angle of incidence, as explained in Section 3.5; an arbitrary $\theta_i < 90^\circ$ can be chosen. Figures 2–4 illustrate the results of power absorption ratio between rough surface and smooth surface. In Figure 2, the results are for a Gaussian correlation function with $h = 1 \mu\text{m}$. The correlation length l varies from 2.0 to 3.0 μm . We note that the absorption ratio increases with frequency. It also increases when the correlation length gets smaller. In Figure 3, the results are repeated for the case of $h = 0.75 \mu\text{m}$. The absorption ratios are smaller than those of Figure 2 because a smaller RMS height gives a smoother surface. In Figure 4, the results are illustrated for surfaces with exponential correlation functions exhibiting larger absorption than surfaces with Gaussian correlation function. The two-media results do not assume any artificial boundary condition and also demonstrate that the absorption depends on all three of the roughness characteristics: RMS height, correlation length, and correlation function. Note that the power due to incoherent scattering vanishes in this case because the wave number k_1 of the lower conductor is much greater than the wave number k of the upper dielectric.

5.2. SPM2 and T-Matrix Comparison

Figure 5 compares 2D SPM2 results with T-matrix results. The modeled surface profiles are Gaussian with $h = 0.48 \mu\text{m}$ and correlation length $l = 1.5 \mu\text{m}$, $l = 2.0 \mu\text{m}$, and $l = 2.5 \mu\text{m}$,

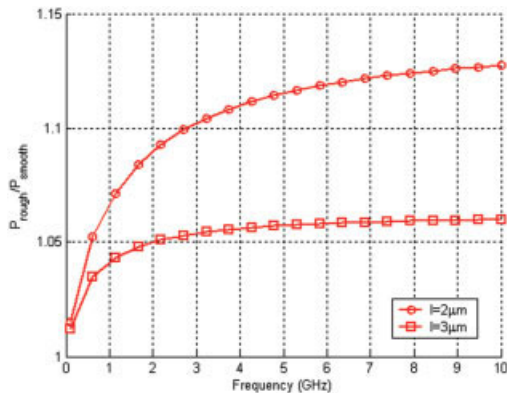


Figure 3 Power absorption ratio: surface with Gaussian correlation function ($h = 0.75 \mu\text{m}$). [Color figure can be viewed in the online issue, which is available at www.interscience.wiley.com]

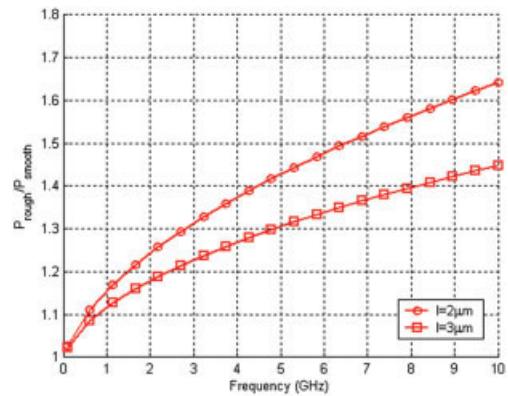


Figure 4 Power absorption ratio: surface with exponential correlation function ($h = 1 \mu\text{m}$). [Color figure can be viewed in the online issue, which is available at www.interscience.wiley.com]

respectively. The numerical T-matrix results are in good agreement with the analytic SPM2 results for rough surfaces of small slope.

5.3. Surface Fields by T-Matrix

The magnetic fields on the conductor surface are calculated numerically by the T-matrix method, for each given rough surface realization. Figure 6 illustrates the magnitude of the magnetic surface field based on one rough surface profile. As normalized by the incident field, the total magnetic field on the surface is close to twice the value of the incident field due to scattering from a well conducting surface. The variation of the surface magnetic field is very small, which is consistent with Morgan's assumption that the surface field is constant.

5.4. SPM2 Two-Media and One-Medium Comparison

In [8], we followed Morgan's assumption by enforcing constant magnetic fields on the rough interface and applied SPM2 only in the conductor region. The power absorption ratio is given by the same closed-form formula as (43). Figure 7 compares the power absorption ratio using two-media SPM2 and the formula based on Morgan's boundary condition. The absorption are illustrated for surfaces with Gaussian correlation function and exponential cor-

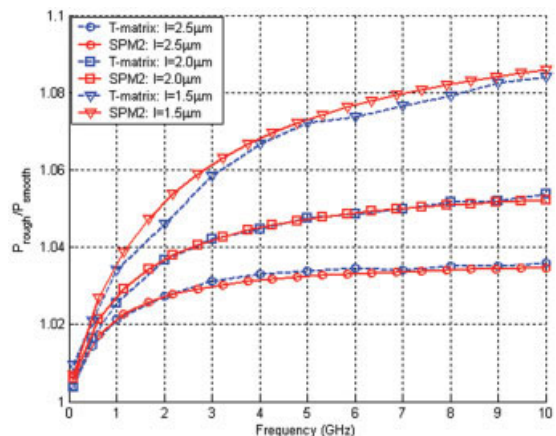


Figure 5 SPM2 versus T-matrix: surface with Gaussian correlation function ($h = 0.48 \mu\text{m}$). [Color figure can be viewed in the online issue, which is available at www.interscience.wiley.com]

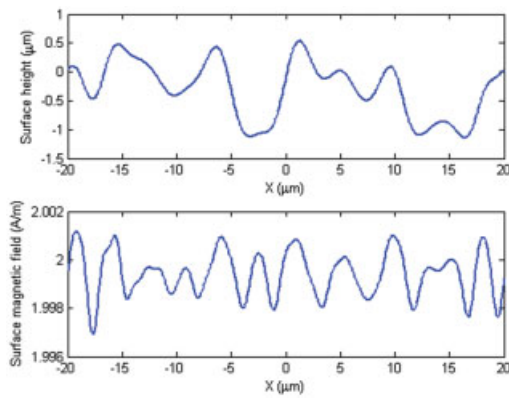


Figure 6 A surface profile and magnitude of surface magnetic fields. [Color figure can be viewed in the online issue, which is available at www.interscience.wiley.com]

relation function ($h = 1 \mu\text{m}$ and $l = 2 \mu\text{m}$). The results are in good agreement between the two methods.

5.5. Emissivity of Soil Surface Using SPM2

Besides calculating power absorption ratio due to the rough interface between a dielectric and a good conductor such as copper, the SPM2 can also be used to solve the emissivity of a less conductive medium, such as soil, in applications of remote sensing. Next we use a common soil profile with Gaussian correlation function ($h = 2.4 \text{ cm}$ and $l = 2 \text{ cm}$). The frequency of the incident plane wave is 5.0 GHz. The relative permittivity of the soil is $15.57 + 3.71i$ and the upper region is air. The emissivity of the soil surface at different incident angles is illustrated in Figure 8. As expected, the emissivity gives the same results as when using the absorptivity formula. Unlike for the copper region, the wave number of the soil medium is comparable to that of the air medium. As a result, the emissivity has contribution from both coherent and incoherent fields scattered by the soil surface. Also note that the emissivity of the soil surface for the exponential correlation function does not exist using SPM2 because of divergent integrals.

6. CONCLUSION

We have applied the 2-D analytic small perturbation method to second order and numerical T-matrix method to study the effects of a random rough surface on power absorption at microwave frequencies. The new methods take into account both dielectric

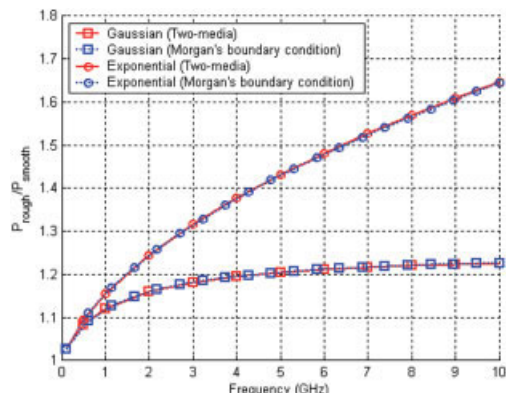


Figure 7 Two-media SPM2 versus one-medium SPM2: $h = 1 \mu\text{m}$ and $l = 2 \mu\text{m}$. [Color figure can be viewed in the online issue, which is available at www.interscience.wiley.com]

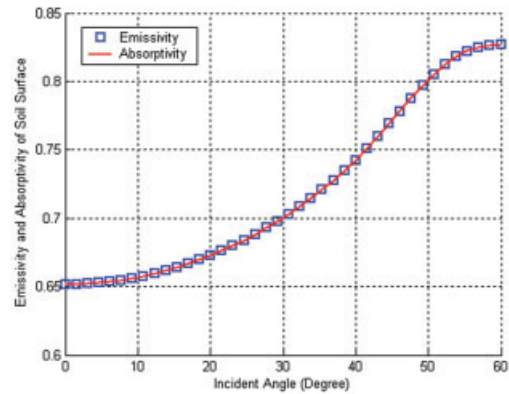


Figure 8 Emissivity and absorptivity versus incident angle: surface with Gaussian correlation function ($h = 2.4 \text{ cm}$, $l = 12.0 \text{ cm}$), $f = 5.0 \text{ GHz}$, and $\hat{\epsilon}_1/\hat{\epsilon}_0 = 15.57 + 3.71i$. [Color figure can be viewed in the online issue, which is available at www.interscience.wiley.com]

and lossy conductive media. The results show the absorption depends on the characteristics of rough surfaces: RMS height, correlation length, and correlation function. Surface magnetic fields are also obtained numerically.

ACKNOWLEDGMENT

The research presented in this paper was supported by Intel Corporation.

REFERENCES

1. S.P. Morgan, Jr., Effects of surface roughness on eddy current losses at microwave frequencies, *J Appl Phys* 20 (1949), 352–362.
2. E.O. Hammerstad and F. Bekkadal, *Microstrip handbook*, ELAB report, University of Trondheim, Norway, 1975, pp. 4–8.
3. A.E. Sanderson, Effect of surface roughness on propagation of the TEM mode, *Advances in Microwaves*, Academic Press, New York, 1971, pp. 1–57.
4. L. Rayleigh, *The theory of sound*, Macmillan, New York, 1929.
5. S.O. Rice, Reflection of electromagnetic waves from slightly rough surfaces, *Commun Pure Appl Math* 4 (1951), 351–378.
6. S.M. Rytov, Yu.A. Kravtsov, and V.I. Tatarskii, *Principles of statistical radiophysics, Vol. 4: Wave propagation through random media*, Springer-Verlag, Berlin, 1989.
7. L. Tsang, J.A. Kong, and R. Shin, *Theory of microwave remote sensing*, Wiley-Interscience, New York, 1985.
8. L. Tsang, X. Gu, and H. Braunisch, Effects of random rough surface on absorption by conductors at microwave frequencies, *IEEE Microwave Wireless Compon Lett* 16 (2006), 221–223.
9. L. Tsang, J.A. Kong, K.-H. Ding, and C.O. Ao, *Scattering of electromagnetic waves, Vol. 2: Numerical simulations*, Wiley Interscience, New York, 2001, pp. 124–151.
10. L. Tsang, J.A. Kong, and K.-H. Ding, *Scattering of electromagnetic waves, Vol. 1: Theory and applications*, Wiley Interscience, New York, 2000, pp. 389–407.
11. W.C. Chew, *Waves and fields in inhomogeneous media*, IEEE Press, New York, 1995, 430–433.

© 2006 Wiley Periodicals, Inc.